# ARTICLES

## Stochastic Simulation of the Electron Radiolysis of Water and Aqueous Solutions

**Simon M. Pimblott* and Jay A. LaVerne**

*Radiation Laboratory, University of Notre Dame, Notre Dame, Indiana 46556*

*Received: February 20, 1997; In Final Form: April 9, 1997*[⊗]

Stochastic modeling of the radiolysis of water and of aqueous solutions employing simulated track structures and the independent reaction times methodology is used to investigate the physical and chemical processes underlying observed radiation chemical kinetics. The calculations accurately reproduce both the time dependent yields of $e_{aq}^-$ and the scavenging capacity dependence of the (scavenged) yields of $e_{aq}^-$, OH, $H_2$, and $H_2O_2$ measured experimentally. The local spatial distribution of $e_{aq}^-$ is described by a Gaussian of standard deviation 4.0 nm. This distribution reflects the "thermalization" of the subexcitation electron. The value matches recent experimental estimates but is somewhat wider than predicted in earlier (deterministic) studies. The Gaussian distribution used for $H_3O^+$, OH, H, and O has a standard deviation of 0.75 nm, which is of the same order obtained previously using deterministic methods. This distribution is due to the distance traveled between electronic collisions of low-energy (<25 eV) electrons and the fragmentation of the molecular cation, $H_2O^+$.

### 1. Introduction

The irradiation of water is immediately followed by a period of fast chemistry whose short-time kinetics reflect the competition between the relaxation of the nonhomogeneous spatial distributions of the radiation-induced reactants and their reactions.[1] A variety of experiments including direct absorption studies[2−8] and treatments involving the inverse Laplace transform analysis of scavenger data[9,10] are available in the literature. These experiments provide a great deal of information about the chemistry occurring and contain the most directly available information about the consequences of radiation damage in water. However, these experiments do not provide sufficient information for a complete understanding of the radiation-induced chemistry. Simulation of the nonhomogeneous kinetics provides insight into the physicochemical processes that determine the initial "local" distribution of reactants and into the factors affecting the competition between the diffusion and the reaction of the radiation-induced reactants. These methods also help in the elucidation of the energy loss properties of electrons in water and of the effects of these processes on the structure and the chemical development of electron tracks.

This study describes the use of stochastic simulation methods to model the short-time radiation chemistry of water and of aqueous solutions of scavengers for the hydrated electron and the hydroxyl radical. The goal is to provide fundamental information that can then be used to aid in the understanding of more complex, complicated chemical and biological systems. A detailed comparison of the results of the calculations with experimental results is made to demonstrate the capabilities of the techniques and to extract information about the local spatial distribution of the radiation-induced reactants and about the reactions underlying the observed chemistry.

### 2. Track Structure Simulation

As an electron passes through an aqueous solution, its energy is transferred primarily to the molecular electrons of the solvent, causing ionization or excitation. Low-energy daughter electrons created in the ionization processes may then produce other ionizations and excitations close to the primary event. The clusters of ionization and excitation events, known as spurs,[11] are usually considered to be spatial isolated, since the mean distance between primary energy loss events along the track of an energetic electron is large; for a 1 MeV electron in liquid water the ratio of the inelastic to the total collision cross section is ∼0.7 and the mean free path between inelastic events is about 0.36 $\mu$m.[12−14]

The energy loss by an energetic electron is an essentially stochastic phenomenon and is therefore amenable to simulation using Monte Carlo techniques. In a recent paper,[14] a methodology for modeling the tracks of energetic electrons was described. This technique models the trajectory of an electron, keeping track of the position, size, and nature of the energy loss events that mark the track of the electron. The calculations reported differ from others in the literature[15−18] in that they employ realistic cross sections for liquid water. In particular, the electronic contribution to the inelastic cross section is derived from the dipole oscillator strength distribution for liquid water and so correctly incorporates the effects of phase in the inelastic energy loss properties, i.e., the cross section is not simply that for density normalized gaseous water.[12] An additional facet is that the outcome of an electronic collision, that is, whether ionization or excitation occurs, is determined from available data for the photoionization of liquid water.[19] The correct experimental angular dependence of the cross section for elastic collisions is employed rather than that suggested by a Rutherford cross section with Moliere screening. The details of the simulation methodology and the cross sections used are described and discussed extensively in the earlier publication.[14]

The excited molecular ions and molecules produced by the transfer of energy from an energetic electron rapidly fragment and thermalize, while low-energy electrons slow, thermalize, trap, and solvate. Consequently, on the picosecond time scale the track of an energetic electron appears as a series of clusters

[⊗] Abstract published in *Advance ACS Abstracts,* July 15, 1997.

S1089-5639(97)00637-3 CCC: $14.00 

of highly reactive radicals and ions. The physicochemical processes following ionization and excitation are poorly understood, and an acceptable theoretical treatment of these events is still required.[1] In the following calculations, the effects of these processes are treated empirically by sampling from Gaussian spatial distributions, which were parametrized to match the experimental data. Track structure simulations have been performed degrading all electrons to a minimum energy, $\gamma_{final}$, of 5 or 25 eV. In the former case, the value of $\gamma_{final}$ is less than the smallest energy loss event that can result in an ionization or an excitation. For $\gamma_{final} = 25$ eV, these processes are still possible and an alternative treatment is necessary. An analytic procedure based on a technique for the prediction of the contents of low-energy spurs outlined by Pimblott and Mozumder[20] has been used. This method relies upon experimentally available photoionization data for liquid water to determine the consequences of an electronic energy loss by an energetic electron. In essence, the probability of an ionization event is determined from the *W* value for liquid water. The *W* value describes the average energy required per ionization and can be estimated from the equation[21]

$$W(E) = EW_{\infty}/(E - U)$$

using the experimentally measured values of $W_{\infty} = 20.8$ eV[7] and $U = 8.3$ eV.[20] Here, $W_{\infty}$ is the limiting *W* value at high energies. For a 25 eV electron, $W(E) \approx 25$ eV and the average number of ionizations is 1. Consequently, for electrons of energy smaller than 25 eV, the average probability of a low-energy ionization event is

$$\langle P_{\text{ionization}}(E)\rangle = E/W(E) = (E - U)/W_{\infty}$$

Complete energy loss simulation to $\gamma_{final} = 5$ eV and simulation to $\gamma_{final} = 25$ eV in conjunction with the use of the analytic treatment for low-energy electrons give (essentially) the same initial track yields. Furthermore, the choice of $\gamma_{final}$ has little effect on the simulated kinetics. The calculations reported here are for the latter approach, i.e., $\gamma_{final} = 25$ eV, since this approach is considerably more computer efficient.

The molecular ions and excited states produced by the energy loss events in the electron radiolysis of liquid water have very short lifetimes even on the time scale of spur kinetics. They fragment or rapidly react with surrounding water molecules, producing the reactive radicals and ions of principle concern in the radiation chemistry of aqueous systems. Recent photoionization experiments have given some information about the kinetics of the thermalization and solvation of low-energy electrons and about the lifetimes of the molecular ions and excited states;[22−26] however, the current state of knowledge about these species is limited even in a qualitative sense.[1] In the following calculations, simple parametrizations are used to describe the outcomes of the various physicochemical processes. This treatment is justified in a discussion of radiation chemical kinetics because the lifetimes of molecular ions, excited states, and presolvated electrons are shorter than 1 ps and are considerably less than the time scale of the experimentally observed nonhomogeneous kinetics.[1]

In the track structure simulations reported, ionization events are identified as one of four main types resulting from the removal of the electron from the $1b_1$, $3a_1$, $1b_2$, or $2a_1$ orbital. The branching ratios for the different ionization events was discussed in the earlier description of the simulation method.[14] In the gas phase, the photoionization of water leads to a variety of different ionic products depending on the available energy;[27] however, here all ionizations are presumed to result in the production of $H_{aq}^+$, OH, and $e_{aq}^-$. This treatment of ionization is common in modeling radiation chemical kinetics[28−30] and relies on the assumption that all single ionization excited ionic states are rapidly converted to the $1b_1$ state before fragmentation. Two different types of excitation event are considered that result in the production of H−OH or $H_2$−O pairs, and the ratio of these pairs is know to be ∼3:1 from the analysis of experimental data.[31]

## 3. IRT Kinetic Method

A high-energy electron in water leaves in its wake a track made up of clusters of highly reactive radicals and ions; $e_{aq}^-$, $H_3O^+$, OH, H, and O. The observed chemistry of these reactants reflects the initial nonhomogeneous spatial distribution and their subsequent diffusion and reaction. Because of the large number of reactants comprising a radiation track, a full random flights simulation of the short-time kinetics in radiolysis is very computer intensive. Alternative, more efficient methodologies are necessary for consideration of the wealth of experimental data available. An elegant Monte Carlo simulation technique, the independent reaction times (IRT) model, has been developed by Clifford et al.,[32−34] which facilitates the modeling of the reaction kinetics of spatially nonhomogeneous distributions of large numbers of particles by using the independent pairs approximation that is implicit throughout the Smoluchowski−Noyes treatment of kinetics.

The IRT model has been developed in detail in a series of papers and has been validated by comparison with full random flights simulations.[32−36] In essence, the simulation of the kinetics of a cluster of reactants begins by considering their initial spatial distribution. The separations between all the pairs of particles are evaluated. Overlapping pairs are allowed to react, and reaction times for all the surviving pairs are calculated from the reaction time distribution functions for the pairs as if they were in isolation (the independent pairs approximation). The resulting ensemble of times is then used to determine the times of subsequent reactions. When a reaction occurs, any reactive products are positioned using the "diffusion approach" detailed by Clifford et al.,[33] new reaction times are determined from the appropriate first passage time distribution function, and a modified ensemble of times is created. The simulation proceeds until a predefined cutoff time is reached or until no reactive particles remain. Repeated realization using a different initial configuration and random number seeds provides the kinetics of the system.

Initially, the IRT method was applied to the kinetics of isolated spurs. Such calculations were used to test the model and the validity of the independent pairs approximation upon which it is based.[32−37] In addition, crude attempts were made to reproduce experimentally measured escape yields using idealized spur size distributions.[38] These calculations predicted physically unrealistic radii for the spurs and, with hindsight, demonstrated that the concept of a distribution of isolated spurs is physically inappropriate. Application of the IRT methodology to an idealized (but inaccurate) radiation track has also been documented,[39] and calculations have now been presented in a number of papers.[30,40,41] Thus far, reasonable agreement between experimental data for scavenger and time-dependent yields and the predictions of kinetic simulation has not been found. Such a match between experiment and calculation is demonstrated in the results reported here, showing that the important input information is the initial configuration of the reactants, i.e., the use of a realistic radiation track structure. A detailed description of the IRT methodology and its application to radiation tracks has been given previously.[39]

**TABLE 1: "Initial"and Short-time Yields of the Radiation-Induced Species Produced by 1 MeV Electrons[c]**

| | | 1 MeV electron track | | 10 keV section of 1 MeV electron track | |
|---|---|---|---|---|---|
| chemical species | expt[a] | "initial" yield | 1 ps yield | "initial" yield | 1 ps yield |
| $e_{aq}^-$ | 4.78 | 4.93 | 4.88 | 4.97 | 4.92 |
| $H_{aq}^+$ | 4.78 | 4.93 | 4.90 | 4.97 | 4.94 |
| OH[b] | 5.50 | 5.37 | 5.57 | 5.41 | 5.60 |
| H | 0.42 | 0.45 | 0.44 | 0.45 | 0.44 |
| $H_2$ | 0.15 | 0.16 | 0.16 | 0.15 | 0.16 |
| O[b] | | 0.16 | | 0.15 | |
| $OH^-$ | | | 0.02 | | 0.02 |
| $H_2O_2$ | | | 0.04 | | 0.04 |

[a] Taken from the analysis of a compilation of scavenger data by LaVerne and Pimblott.[9] Similar values were also obtained by Schwarz.[31] [b] Reaction of "O" atom with water to give 2OH radicals is (effectively) instantaneous on the time scale of spur reaction. [c] The initial yield is defined arbitrarily as the yield after all the physicochemical processes have taken place and before chemistry occurs.

The predicted kinetics reported in this study are for the degradation of an electron of initial energy of 1 MeV by 10 keV, including the complete simulation of any high-energy $\delta$ rays produced (even if their energy is greater than 10 keV). Each calculation represents the averaged chemistry of at least $10^2$ *different* electron tracks. The reaction scheme and IRT reaction parameters for the radiolysis of water as well as the diffusion parameters employed in the kinetic calculations are taken from Tables 1 and 2 of ref 42. In the scavenger studies, generic idealized scavengers are considered, although the parameters used are appropriate for the prototypical $e_{aq}^-$ scavenger methyl chloride and the OH scavenger bromide.

## 4. Results and Discussion

**4.1. Ionization and Excitation Yield**. The ionization yields predicted by the simulation technique for a 1 MeV electron track and for the first 10 keV of attenuation of a 1 MeV electron track are both 4.9(2) per 100 eV with track-to-track fluctuations of $\pm 0.01$ and $\pm 0.2$, respectively. (Radiation chemical yields are given in units ($G$ values) of radicals or molecules per 100 eV of energy absorbed.) This value is in excellent agreement with the initial yields extrapolated from direct absorption experiments that measure the time dependence of the hydrated electron, $G_0 = 4.9$,[7,43] and from studies of the scavenging capacity dependence of the scavenged yield of the electron, $G_0 = 4.8$.[9] The yield of electronic excitation predicted by the simulations is 1.8, which compares favorably with earlier calculations of Kaplan et al.[44] that predicted 1.4. This yield for excitation is somewhat larger than expected from the initial yield of hydrogen atom and molecular hydrogen, $G(H + H_2) = 0.6$, inferred from scavenger experiments.[9] However, this difference is probably due to the effects of cage recombination. When these effects are included as suggested by Pimblott and Mozumder,[20] the excitation yield is reduced to 0.6 and the predicted excitation yield corresponds to that obtained experimentally.

The "initial" physicochemical and 1 ps yields of the radiation-induced reactants resulting from the ionization and excitation yields are given in Table 1. The agreement between these calculated yields and the yields obtained by extrapolation of experimental data to short times[9] is excellent with errors for the radical species smaller than 2%. Comparison of the yields for 1 MeV electron tracks and for the first 10 keV section of these tracks shows that the short-time yields are essentially the same, which suggests that the 10 keV section is an acceptable model for the complete track. Reaction in the first picosecond following irradiation accounts for a chemically insignificant amount of the radiation-induced radicals.

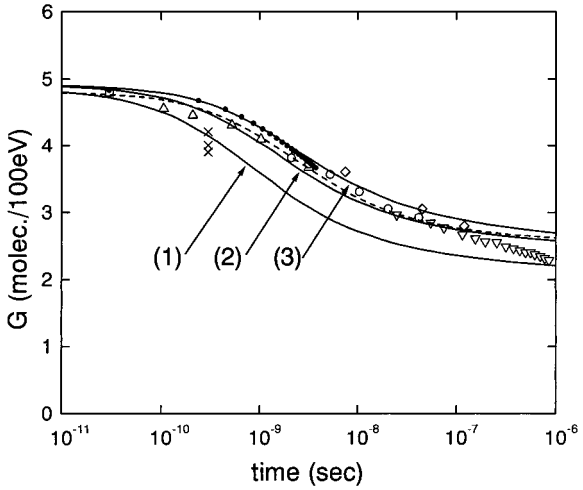


**Figure 1.** Time-dependent decay kinetics of $e_{aq}^-$ in the electron radiolysis of water. Direct absorption experiments: ref 2 (◇); ref 3 (▽); ref 5, stroboscopic detection method (△); ref 5, CW laser/photodiode detection method (○); ref 7 (□); ref 8 (×); ref 45 (●). ILT of scavenger data of ref 43 are shown as the dashed line. IRT simulation results with $\sigma(OH) = 0.75$ nm are shown as solid lines for $\sigma(e_{aq}^-) = 3.0$ nm (1), $\sigma(e_{aq}^-) = 4.0$ nm (2), and $\sigma(e_{aq}^-) = 5.0$ nm (3).

**4.2. Hydrated Electron Yield**. A large amount of experimental data concerning the radiation chemical yield of $e_{aq}^-$ is available in the literature; direct absorption experiments have been used to measure the time dependence of the yield in deaerated water[2,3,5−7,45] and a variety of scavengers have been used to determine the effect of scavenging capacity, $s$ (equal to the product of the scavenger concentration and the rate coefficient for the scavenging reaction, $k$[S]), on the scavenged yield of $e_{aq}^-$.[9,46−49,50,51,52] The time dependence of $e_{aq}^-$ measured experimentally is shown in Figure 1. Extrapolation of these data to the picosecond time scale suggests a yield of $e_{aq}^-$ of $4.9 \pm 0.2$.[43] These data are compared with data from simulated kinetics of a 1 MeV electron degraded by 10 keV. Three different calculations are shown in which the standard deviation of the "thermalization" distribution for $E = \gamma_{final}$ to solvation of $e_{aq}^-$ is 3.0, 4.0, and 5.0 nm. In all three sets of simulations the standard deviation of the spatial distribution of the "heavy reactants" ($H_3O^+$, OH, H, and O) is 0.75 nm. The best agreement between experiment and calculation is found for $\sigma(e_{aq}^-) = 4.0$ nm. Additional simulations (not shown) reveal that the time dependence of $e_{aq}^-$ is not very sensitive to the width of the distribution for OH, provided the parameter $\sigma$(OH) is in the range 0.5−1.0 nm. The kinetics predicted at short times, less than 0.1 ns where very little reaction occurs, are primarily determined by the ionization yield. This parameter is determined in the Monte Carlo track structure simulation and is not adjusted in any manner whatsoever.

The "thermalization" distribution for $e_{aq}^-$ represents the degradation of the electron energy from $E = \gamma_{final}$ to solvation. The width of this distribution is in very good agreement with estimates of Crowell and Bartels in a recent picosecond laser study of the multiphoton ionization of liquid water. For energies greater than 12 eV they find a lower limit to the thermalization distance of $\sigma(e_{aq}^-) > 3.5$ nm.[53] Furthermore, the root-mean-square distance, $\langle r^2 \rangle^{1/2} = \sigma\sqrt{3}$, obtained from the Gaussian distribution is 6.9 nm, which is similar to the mean thermalization lengths estimated by Konovalov et al. from electron photoejection experiments in water, $\langle l \rangle = 6.0-8.0$ nm.[54,55] It is important to note that the thermalization distances of Konovalov

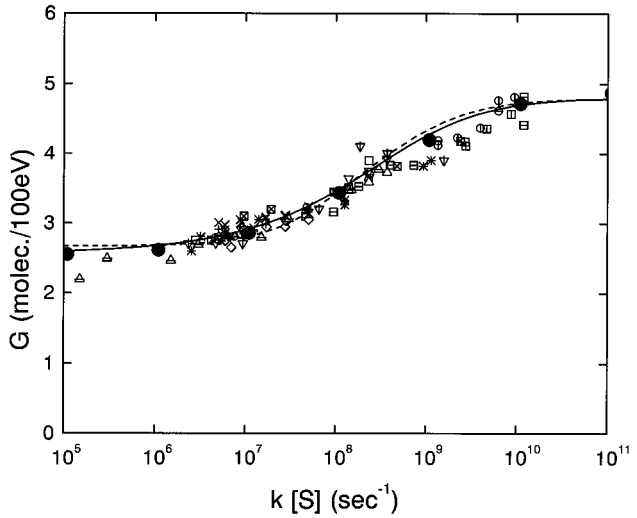


**Figure 2.** Scavenging capacity dependence of the scavenged yield of $e_{aq}^-$. Scavenger experiments: ref 46, MeCl (□), MeCl + $10^{-3}$ M MeOH (○), MeCl + $10^{-2}$ M MeOH (△), MeCl + $10^{-1}$ M MeOH (▽); ref 49, MeCl + $10^{-2}$ M PrOH (◇), MeCl + $3 \times 10^{-2}$ M PrOH (+), MeCl + $10^{-1}$ M PrOH (×); ref 50, $N_2O$ (*); ref 51, $N_2O$ (▽ with a vertical slash); ref 52, $Cd^{2+}$ (□ with × crossbar); ref 47, conventional pulse radiolysis with $Cd^{2+}$ (□ with horizontal slash), cystamine (○ with horizontal slash), stroboscopic pulse radiolysis with $Cd^{2+}$ (□ with vertical slash), cystamine (○ with vertical slash); ref 48, glycylglycine (△ with horizontal slash). Best fit to scavenger data with $G_{esc} = 2.56$, $G_0 = 4.80$, and $\tau = 2.77$ ns[43] (solid line). The Laplace transform of direct absorption data from ref 43 is shown as a dashed line. IRT simulation with $\sigma(e_{aq}^-) = 4.0$ nm and $\sigma(OH) = 0.75$ nm (●).

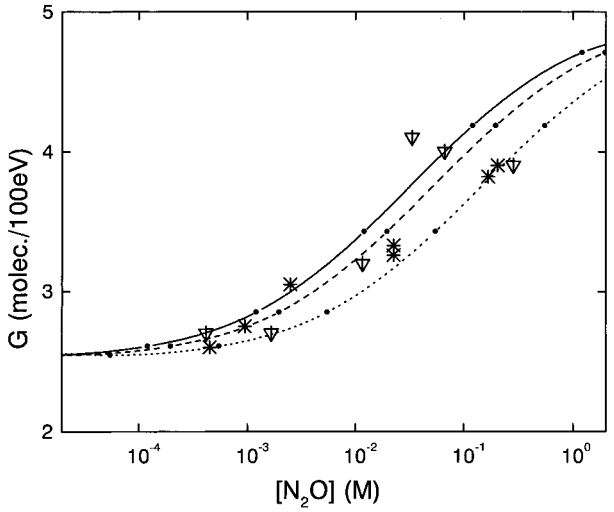


**Figure 3.** Effect of $N_2O$ concentration on the yield of $N_2$ produced by electron radiolysis. Experiments: ref 50, $N_2O$ (*); ref 51, $N_2O$ (▽ with a vertical slash). IRT simulation with $k(e_{aq}^- + N_2O) = 2.0 \times 10^9$ $M^{-1}$ $s^{-1}$ (solid line), $k(e_{aq}^- + N_2O) = 5.6 \times 10^9$ $M^{-1}$ $s^{-1}$ (dashed line), and $k(e_{aq}^- + N_2O) = 9.1 \times 10^9$ $M^{-1}$ $s^{-1}$ (dotted line).

et al. depend on the initial electron energy, whereas the width obtained here is for a distribution of energies. Previous theoretical studies are rather contradictory and do not match the available experimental data. Consequently, agreement with the calculations reported here is limited; the spur width is considerably larger than obtained from deterministic analyses of scavenger experiments, where $\sigma(e_{aq}^-) \approx 2-3$ nm,[31] while the $\langle r^2 \rangle^{1/2}$ distance is still considerably smaller than the "average thermalization distance" of ~13 nm estimated by Monte Carlo simulation of the energy loss of subexcitation electrons in solid water[56−58] using the cross sections for ice.[59−61] To be fair, in the discussion of the latter paper, the authors document considerable uncertainties in their calculations and note that their simulated distribution has a most probable separation distance of about 2.5 nm but with a very long tail. The Gaussian function employed here is a convenient empirical distribution and the profile may not be entirely realistic at short times; however, because of the nature of Brownian motion, the actual distribution will rapidly tend to a Gaussian as diffusion occurs.

Theoretical studies[9,62−64] have previously shown that the time dependent decay of $e_{aq}^-$, $G(t)$, and the dependence of the scavenged yield of $e_{aq}^-$ on scavenging capacity, $G(s)$, are related by the Laplace transform relationship,

$$G(s) = s\int_0^\infty G(t) \exp(-st)\, dt \qquad (1a)$$

Until recently, there was an apparent discrepancy between the two types of experiment.[9,65] The origins of the differences between the sets of data were revisited in ref 43, and the data have been reconciled by the use of an improved measurement for the rate coefficient for the scavenging of $e_{aq}^-$ by $CH_3Cl$.[49] Clearly, an accurate description of the radiation chemistry of water must reproduce both types of experimental data using the same parameters.

Figure 2 shows the scavenging capacity dependence of the scavenged yield of $e_{aq}^-$ calculated with $\sigma(e_{aq}^-) = 4.0$ nm and $\sigma(OH) = 0.75$ nm. Comparison of the modeled chemistry with data from experimental scavenger studies and with the scavenging capacity dependence predicted by the Laplace transform of the time dependent data reported by Pimblott et al.[43] shows excellent agreement. The calculations reproduce both the absolute yields and the relative variation as a function of scavenging capacity of the majority of the data. The experimental yields in the figure are used as given in the original studies. For the most part, the scavenging capacities of the solutions were calculated using rate coefficients from the compilation of Buxton et al.[66] with corrections to the scavenging rate coefficient for ionic strength and concentration effects made using experimental determinations of $k(e_{aq}^- + S)$ where feasible. (This correction is particularly important for concentrated solutions. For instance, the rate coefficient for cystamine with $e_{aq}^-$ drops from $3.2 \times 10^{10}$ $M^{-1}$ $s^{-1}$ at 0.1 M to $0.7 \times 10^{10}$ $M^{-1}$ $s^{-1}$ at 1 M.)

Two scavenging rate coefficients are not taken from ref 66. (i) For $e_{aq}^- + N_2O$, experimental estimates of the rate coefficient for the reaction of $e_{aq}^-$ with $N_2O$ range from $\sim 0.2 \times 10^{10}$ to $1.0 \times 10^{10}$ $M^{-1}$ $s^{-1}$.[67−72] This difference represents a factor of 5 in the scavenging capacity dependence and makes it difficult to properly collate this system with the experimental data for other systems. The selected value in ref 66 for this reaction is $9.1 \times 10^9$ $M^{-1}$ $s^{-1}$, which is at the upper end of the measured range and is considerably different from that selected in the earlier compilation of Anbar and Neta,[73] where $k(e_{aq}^- + N_2O) = 5.6 \times 10^9$ $M^{-1}$ $s^{-1}$. Experimental data for the effect of $N_2O$ concentration on the yield of $N_2$ are shown in Figure 3. Also included in the figure are calculations for the system employing scavenging rate coefficients of 2.0, 5.6, and $9.1 \times 10^9$ $M^{-1}$ $s^{-1}$. Clearly, the best agreement of simulation with experiment is obtained for $k(e_{aq}^- + N_2O)$, which is $5.6 \times 10^9$ $M^{-1}$ $s^{-1}$ as measured by Hart and Fielden[70] and given in the compilation of Anbar and Neta. Furthermore, a rate coefficient of $\sim 5 \times 10^{10}$ $M^{-1}$ $s^{-1}$ is also obtained from the measurement of $k/G$ by Koulkes et al.[74] at $[N_2O] = 0.022$ M if the $G$ value of Dainton and Logan[50] (~3.3) is assumed. Consequently, the data for $N_2O$ are presented in Figure 2 using $k(e_{aq}^- + N_2O) = 5.6 \times 10^9$ $M^{-1}$ $s^{-1}$. The considerable scatter in the data shown in Figure 3 makes it impossible to distinguish if the choice of $k(e_{aq}^- + N_2O)$ is closer to the correct value than that given by Buxton et

al. or if other factors are involved.[66] (ii) For $e_{aq}^- + CH_3Cl$, as discussed earlier, the recent measurement of Schmidt et al.[49] was used for this scavenging reaction.

Figure 2 contains significantly more data than Figure 5 of ref 9 and Figure 2 of ref 43. The data of Wolff et al.[47] for the scavengers $Cd^{2+}$ and cystamine extends the range of scavenging capacity from $\sim 10^9$ $s^{-1}$ to greater than $10^{10}$ $s^{-1}$. The conventional pulse radiolysis experiments (symbols □ and ○ with horizontal slashes) are based on dosimetry assuming the $e_{aq}^-$ yield at 100 ns is ~2.8, which is consistent with the time dependence shown in Figure 1. The 6 ns integrated yields obtained by stroboscopic pulse radiolysis (symbols □ and ○ with vertical slashes) rely on dosimetry using the nanosecond time scale decay of $e_{aq}^-$ measured by Jonah et al.,[6] which is also included in Figure 1 and is reproduced by the track structure simulation. The data for $Cd^{2+}$ at high scavenging capacity (□ with horizontal and vertical slashes) mesh closely with additional studies at lower scavenging capacity by Shirashi et al.[52] (□ with × crossbars).

One of the $e_{aq}^-$ scavengers considered in Figure 2, cystamine, is also a very potent OH scavenger with a rate coefficient, $k$(OH + S), of $\sim 2 \times 10^{10}$ $M^{-1}$ $s^{-1}$.[66] The effects of cooperative scavenging of OH on the amount of $e_{aq}^-$ scavenged have been shown to be significant when the scavenging capacity for $e_{aq}^-$ is low and when that for OH is high, $\Delta G \approx 0.3$.[75] However, at the high $e_{aq}^-$ scavenging capacities of the data included in Figure 2, the cooperative effect of cystamine scavenging of OH on the yield of $e_{aq}^-$ is very small. The appropriate correction is straightforward to calculate using the analytic formalism presented in ref 75. At an $e_{aq}^-$ scavenging capacity of $10^8$ $s^{-1}$, the cooperative effect of cystamine scavenging of OH results in an increase of 1.2% in the scavenging yield of $e_{aq}^-$, while at $10^{11}$ $s^{-1}$ the increase is 0.2%. These are not experimentally distinguishable differences.

Also included in Figure 2 is the fit of the empirical function[9]

$$G(s) = G_{esc} + (G_0 - G_{esc})\left(\frac{(\tau s)^{1/2} + (\tau s)/2}{1 + (\tau s)^{1/2} + (\tau s)/2}\right) \quad (2a)$$

to the experimental data for $CH_3Cl$ and glycylglycine obtained by Pimblott et al.[43] The parameters $G_0$ and $G_{esc}$ are the initial yield and that escaping spur reaction, respectively, and $\tau$ is a time constant characteristic of the nonhomogeneous reaction. This fit was obtained with $G_0 = 4.80$, $G_{esc} = 2.56$, and $\tau = 2.77$ ns. The inverse Laplace transform of eq 2 for $G(t)$ is[9]

$$G(t) = G_{esc} + 2(G_0 - G_{esc})F_f\left(2\left(\frac{t}{\pi\tau}\right)^{1/2}\right) \quad (3)$$

with $F_f(x)$ being the auxilliary function for the Fresnel integrals.[76] The decay kinetics predicted by this analysis are shown in Figure 1 and are in excellent agreement with the modeled kinetics as well as with results from the direct absorption experiments.[43]

The only discrepancy between the calculated $e_{aq}^-$ yields and the experimental values are for some of the scavenging data for $N_2O$, as discussed above, and the direct absorption measurement of Hunt and co-workers[8] in deaerated water. The studies of Hunt showed no decay in the yield of $e_{aq}^-$ from 20 to 350 ps, and it was inferred that the initial yield of $e_{aq}^-$ was 4.0.[77] Higher yields measured on the same time scale with scavengers[47] were attributed to scavenging of the dry electron. Recent subpicosecond laser studies[22,26] have shown that the electron is solvated within a few tenths of a picosecond, so this type of dry electron reaction cannot be occurring (unless the rate coefficient is about $10^{14}$ $M^{-1}$ $s^{-1}$). There is no obvious reason why the early work of Hunt and co-workers on the decay of $e_{aq}^-$ in deaerated water is flat on the subnanosecond time scale. In this modeling study, more weight has been given to the recent studies of Jonah and co-workers[45] and of Sumiyoshi et al.[7]

The decay of $e_{aq}^-$ in deaerated water is due to a number of spur reactions, the most important being[31]

$$e_{aq}^- + H_3O^+ \rightarrow H \quad k = 2.3 \times 10^{10}\ M^{-1}\ s^{-1} \quad (R1)$$

and

$$e_{aq}^- + OH \rightarrow OH^- \quad k = 3.0 \times 10^{10}\ M^{-1}\ s^{-1} \quad (R2)$$

The calculations show the time dependence of these two reactions to be the same; however, the yields differ by a factor of about 2. At 1 ps, $G$(R1) ≈ 0.01 and $G$(R2) ≈ 0.02, while at 1 ns $G$(R1) ≈ 0.25 and $G$(R2) ≈ 0.52, and at 1 μs $G$(R1) ≈ 0.63 and $G$(R2) ≈ 1.24. The rate coefficients of the two reactions differ by less than 8%,[66] and in the simulations the initial distributions describing the separation between sibling $e_{aq}^- - H_{aq}^+$ and $e_{aq}^- - OH$ pairs are the same, a Gaussian with standard deviation $\sigma = (\sigma^2(e_{aq}^-) + \sigma^2(OH))^{1/2} \approx 4.1$ nm. The different yields for the two reactions reflect the different rates of reaction between sibling pairs due to the effective reaction distances of $e_{aq}^- + H_{aq}^+$, $a_{eff} = 0.23$ nm, and of $e_{aq}^- + OH$, $a_{eff} = 0.54$ nm. The large value of the diffusion coefficient of $H_{aq}^+$, $D = 9.0 \times 10^{-9}$ $m^2$ $s^{-1}$, boosts the rate of reaction R1, so it is comparable to that for reaction R2.

**4.3. Molecular Hydrogen Yield**. Although reactions R1 and R2 dominate the decay kinetics of $e_{aq}^-$, it is also involved in additional chemistry. Two of these reactions

$$e_{aq}^- + e_{aq}^- \rightarrow H_2 + 2OH^- \quad 2k = 1.1 \times 10^{10}\ M^{-1}\ s^{-1} \quad (R3)$$

$$e_{aq}^- + H \rightarrow H_2 + OH^- \quad k = 2.5 \times 10^{10}\ M^{-1}\ s^{-1} \quad (R4)$$

as well as the bimolecular reaction of H,

$$H + H \rightarrow H_2 \quad 2k = 1.55 \times 10^{10}\ M^{-1}\ s^{-1} \quad (R5)$$

give molecular hydrogen. Although the time dependence of the production of $H_2$ has not been measured, the effect of scavenging capacity on the yield of $H_2$ has been studied experimentally.[9,78−80] The yield of $H_2$ in the electron radiolysis of deaerated water is considered in Figure 4. It compares the experimental data for the scavenging capacity dependence of $H_2$ with the simulated yields from a 10 keV section of a 1 MeV track. The agreement between calculation and experiment is good; however, there are some small differences. The calculations correctly predict the small $s$ yield and chart the relative decrease in the yield of $H_2$ as a function of $s$. There is an error of up to 20% in the yield, which is equivalent to a factor of ~2 in the absolute scavenging capacity dependence for $s$, in the range $10^7 - 10^9$ $s^{-1}$. The origins of this discrepancy are unclear, although it may in part be due to the fact that the calculations include an initial unimolecular production of $H_2$ of 0.15 molecules/100 eV. This initial yield appears to be somewhat higher than suggested experimentally. In fact, the experimental data in Figure 4 might be taken to imply the absence of an "initial" $H_2$ yield.[80] Gas phase information shows that $H_2$ is formed by both ionization and excitation of isolated water molecules.[27,81,82] Furthermore, in the interpretation of the radiolysis data at high $s$, it must also be remembered that in these high-molarity solutions, the local environment of a water molecule is not the same as in pure water. A variety of effects

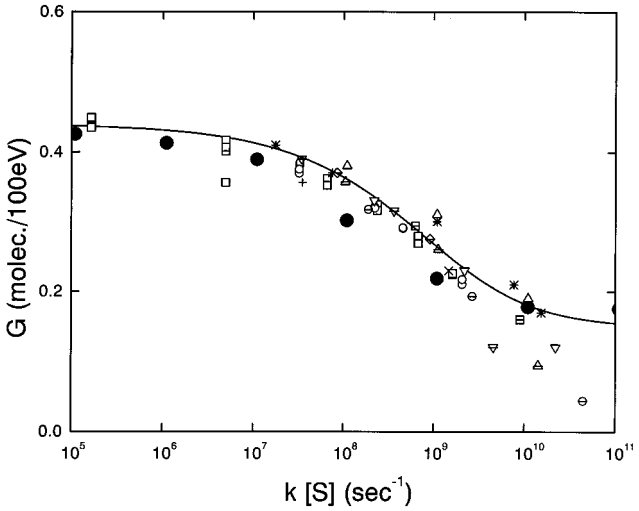


**Figure 4.** Scavenging capacity dependence of the yield of $H_2$. Scavenger experiments: ref 78, $NO_2^-$ (□), $Cu^{2+}$ (○); ref 79, $H_2O_2$ (*); ref 80, $H_2O_2$ (△), acrylamide (▽), $Cr_2O_7^{2-}$ (□ with horizontal slash), $CrO_4^{2-}$ (○ with horizontal slash), $NO_3^-$ (△ with horizontal slash), $BrO_3^-$ (▽ with horizontal slash), $IO_3^-$ (◇ with horizontal slash), $Fe(CN)_6^{3-}$ (+), $S_2O_3^{2-}$ (×). Best fit to scavenger data with $G_{esc} = 0.44$, $G_0 = 0.15$, and $\tau = 0.47$ ns[9] (solid line). IRT simulation with $\sigma(e_{aq}^-) = 4.0$ nm and $\sigma(OH) = 0.75$ nm (●).

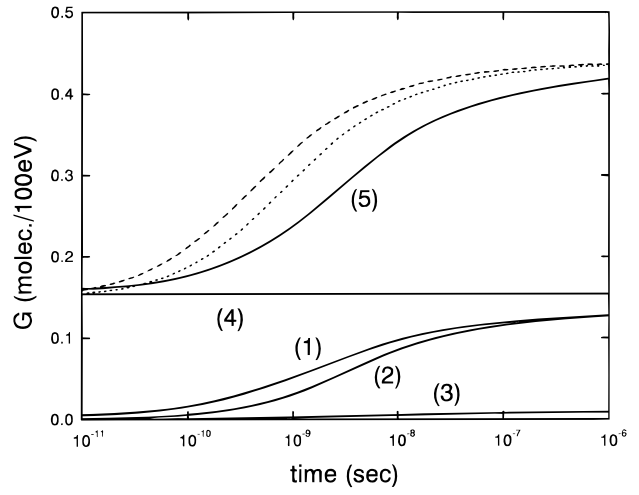


**Figure 5.** Time dependent formation of $H_2$ in the electron radiolysis of water. ILT of best fit to scavenger data with $G_{esc} = 0.44$, $G_0 = 0.15$, and $\tau = 0.47$ ns[9] using $s$ as the Laplace variable (dotted line) and using $p$ (=2$s$) as the Laplace variable (dashed line). IRT simulation with $\sigma(e_{aq}^-) = 4.0$ nm and $\sigma(OH) = 0.75$ nm shown as solid lines labeled as follows: $G(e_{aq}^- + e_{aq}^-)$ (1); $G(e_{aq}^- + H)$ (2); $G(H + H)$ (3); $G$(unimolecular $H_2$) (4); $G$(total $H_2$) (5).

not included in the calculations may facilitate deactivation of the excited states leading to $H_2$.

Figure 5 shows the modeled formation kinetics for $H_2$ in deaerated water. In neutral water, the $H_2$ produced by nonhomogeneous reaction comes equally ($G = 0.13$) from reactions R3 and R4 with the bimolecular reaction of H atoms making almost no contribution to the total yield ($G \approx 0.01$). The time dependences of the $H_2$ formation via reactions R3 and R4 are very different; the former is the more rapid even though ($2 \times k$(R3)) is only about 20% of $k$(R4).[66] The difference reflects the much smaller initial yield of H ($G = 0.4$) compared to $e_{aq}^-$ ($G = 4.9$) and its formation via reaction

$$e_{aq}^- + H_3O^+ \rightarrow H \qquad \text{(R6)}$$

on the spur time scale. At all times in the nonhomogeneous evolution of the radiation track, the concentration of $e_{aq}^-$ is much greater than that of H.

It has been suggested that the "experimental time dependent formation kinetics" for molecular hydrogen can be obtained from the scavenger data shown in Figure 3 using a Laplace transform relationship similar to that given above for $e_{aq}^-$.[10] Since the scavenging of either of a pair of reacting electrons prevents $H_2$ formation, the scavenging capacity for $H_2$ is assumed to be twice the scavenging capacity of the solution for $e_{aq}^-$, i.e., $p = 2k$[S]. Consequently, the Laplace transform variable is $2k$[S] rather than $k$[S] and

$$G(p) = p\int_0^\infty G(t)\exp(-pt)\,dt \qquad \text{(1b)}$$

The data in Figure 3 can be described by the empirical function[9]

$$G(p) = G_{esc} + (G_0 - G_{esc})\left(\frac{(\tau p)^{1/2} + (\tau p)/2}{1 + (\tau p)^{1/2} + (\tau p)/2}\right) \qquad \text{(2b)}$$

where $G_0 = 0.15$, $G_{esc} = 0.44$, and $\tau = 0.47$ ns. Thus, the time dependent formation kinetics are given by eq 3 with these parameters.

The formation kinetics predicted by this inverse Laplace transform analysis are also shown in Figure 5. They are somewhat faster (about an order of magnitude) than the modeled formation kinetics. This discrepancy has several sources. First, there is a slight discrepancy, mentioned earlier, between the calculated and experimental scavenger data shown in Figure 3. This difference, about 20% in yield or a factor of 2 in scavenging capacity, would not account for the observed discrepancy. More important is the fact that the inverse Laplace method makes the assumption that all the $H_2$ is formed via the bimolecular reaction of $e_{aq}^-$. A significant fraction of $H_2$ is formed by reaction R4, and this route is somewhat slower for the reasons discussed earlier. Finally, the simulations reported refer to a 10 keV section of a 1 MeV track and so ignore the effects of track ends. Short tracks account for about 29% of the energy loss events of a 1 MeV electron,[12,13] and the short-time chemistry of these more densely concentrated regions of reactants is somewhat different from that of spurs and blobs. Calculations in progress suggest this effect may be particularly significant for the yield of $H_2$, since the formation of $H_2$ is due to reactions R3 and R4, which involve the encounter of reactants from different (separate) electronic energy loss events. In contrast, the effect of track ends on the kinetics of $e_{aq}^-$ is less significant, since the decay of $e_{aq}^-$ is dominated by reactions R1 and R2, which are reactions of (predominantly) sibling species.

**4.4. Hydroxyl Radical Yield**. Although the absolute yield of $e_{aq}^-$ and its time dependent decay kinetics in deaerated water are well-known experimentally, this is not the case for the OH radical. Only limited information about the time dependence of the OH yield in water is available. Jonah and co-workers have made two attempts to perform direct absorption measurements over the time scale 200 ps to 3 ns.[4,45] Over this time period, the yield of OH radical decays by about 27%. Absolute yields were not reported in the later paper, ref 45, and the values quoted in the earlier study are of limited precision (C. D. Jonah, personal communication). To make matters worse, application of the inverse Laplace transform technique to the scavenger data is not without problems. Even though there is a great wealth of scavenger experiments for OH in aerated systems, there is a large amount of scatter in the data for the effects of scavenging capacity when different scavengers are considered. The scavenger experiments suggest that $G_{esc} \approx 2.5-2.6$ and $G_0 \approx 5.5$. However, for the data of Schuler and Behar,[83] which employ

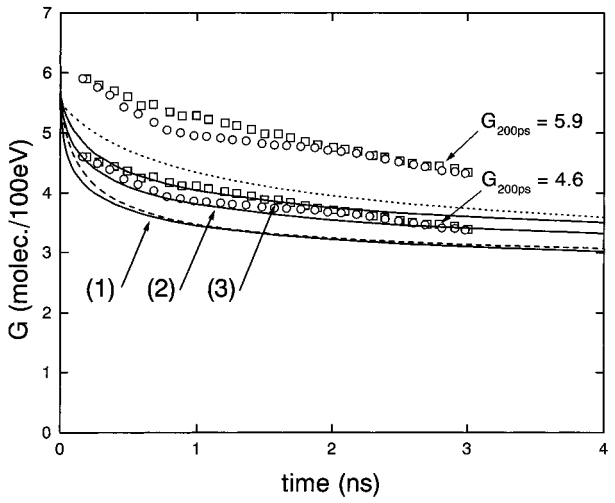


**Figure 6.** Time dependent decay kinetics of OH in the electron radiolysis of water. Direct absorption experiments: ref 4 (□); ref 45 (○). ILT of scavenger data are as follows: $HCO_2^-/HCO_2H$ data[84−88] (dotted line); $Fe(CN)_6^{4-}$ data[83] (dashed line). IRT simulations with $\sigma(e_{aq}^-) = 4.0$ nm are shown as solid lines labeled as follows: $\sigma$(OH) = 0. 5 nm (1); $\sigma$(OH) = 0.75 nm (2); $\sigma$(OH) = 1.0 nm (3).

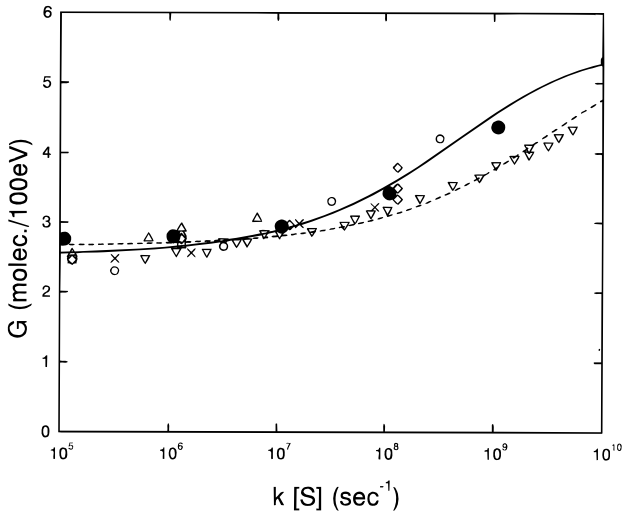


**Figure 7.** Scavenging capacity dependence of the scavenged yield of OH. Scavenger experiments: ref 84, $HCO_2H$ (◇); ref 85, $HCO_2H$ (△), $HCO_2^-$ (×); ref 83, $Fe(CN)_6^{4-}$ (▽); ref 87, $HCO_2H$ (○); ref 88, $HCO_2H$ (□). Best fit to scavenger data is as follows: $HCO_2^-/HCO_2H$ data (solid line); $Fe(CN)_6^{4-}$ data (dashed line). IRT simulation with $\sigma(e_{aq}^-) = 4.0$ nm and $\sigma$(OH) = 0.75 nm for aerated solution (●).

$Fe(CN)_6^{4-}$ as the OH scavenger, the best fit value of $\tau$ in the empirical function (eq 2a) is 0.26 ns, while for the data of refs 84−87, which use $HCO_2^-$ or $HCO_2H$, $\tau$ = 1.67 ns. This difference is equivalent to a factor of about 7 on the time scale of the time dependent decay kinetics of OH in water.

The experimental decay kinetics of OH suggested by the direct absorption measurements[4,45] and scavenger data are shown in Figure 6. The time dependence of the OH decay curve measured by direct absorption more closely resembles that predicted by the inverse Laplace transform analysis of the $HCO_2^-/HCO_2H$ data than that of the $Fe(CN)_6^{4-}$ data. However, realistically, it is not possible to make a distinction, since the two decay curves are very similar and the scatter between the two sets of absorption data is significant. Also included in Figure 6 are the predictions of three kinetic simulations in which $\sigma(e_{aq}^-)$ is 4.0 nm and $\sigma$(OH) is 0.5, 0.75, and 1.0 nm. The choice of a value of $\sigma$(OH) in the range 0.5−1.0 nm does not affect the predicted kinetics of $e_{aq}^-$ (or $H_2$). However, it does have a significant effect upon the modeled chemistry of OH. The use of $\sigma$(OH) = 0.5 nm matches the inverse Laplace transform of the $Fe(CN)_6^{4-}$-scavenged yields, whereas a larger value ($\sigma$(OH) = 0.75 or 1.0 nm) is necessary to reproduce the $HCO_2^-/HCO_2H$ data and the curvature from the direct absorption experiments.

Figure 7 compares the predictions of kinetic simulations on a 10 keV section of a 1 MeV electron track for the effect of scavenger on the scavenged yield of OH with experimental data. The simulations are for distributions with $\sigma(e_{aq}^-) = 4.0$ nm and $\sigma$(OH) = 0.75 nm. The calculated yields pass between the sets of experimental data using $Fe(CN)_6^{4-}$ as the OH scavenger and those using $HCO_2^-$ or $HCO_2H$. The chemistry of OH in water is dominated by reactions R2 and

$$OH + OH \rightarrow H_2O_2 \qquad (R7)$$

which contribute almost equally to the removal of OH, with calculated microsecond $G(\Delta OH)$s of 1.2 and 1.6, respectively. The time dependences of reactions R2 and R7 are very different with reaction R7 taking place on the 0.1−1 ns time scale and reaction R2 on the 1−10 ns time scale. The different kinetics of the reactions result in two components to the decay of OH. This contrasts with $e_{aq}^-$, where reactions R1 and R2 occur on virtually the same time scale.

**4.5. Hydrogen Peroxide Yield**. In contrast to the scavenger studies of OH, there is remarkable consistency in the data obtained in experiments examining the effect of scavenging capacity for OH on the yield of $H_2O_2$. Figure 8 shows the scavenger data available for experiments performed at pH 2 and at pH 7.[89−94] For the most part, the data at pH 2 are for experiments with $Br^-$ as the scavenger for OH, while at pH 7 two different types of OH scavenger, halide ions ($Br^-$ and $Cl^-$) and ethanol, are considered. Included in the figures are the predictions of simulations for the effect of $Br^-$ on the $H_2O_2$ yield from a 10 keV section of a 1 MeV track with $\sigma(e_{aq}^-)$ = 4.0 nm and $\sigma$(OH) = 0.75 nm. At pH 2, the simulations are in excellent agreement with the experimental data, matching both the small *s* limiting yield, $G_{esc}$, and the absolute scavenging capacity dependence. Agreement is also very good at pH 7, although here there is a slight discrepancy in the scavenging capacity dependence for large *s*. This discrepancy is due to differences between the experimental and theoretical conditions.

In Figure 8b, the data for large *s* are from experiments in which ethanol was used as the OH scavenger.[93] The time dependent rate coefficient of a diffusion-limited reaction has the form

$$k(t) = k(\infty)(1 + \beta/\sqrt{t}) \qquad (4)$$

where $\beta = k(\infty)/(4\pi D')^{3/2}$ with $D'$ being the relative diffusion coefficient of OH and the scavenger.[95,96] The time dependence of the rate coefficient is a misnomer and arises from the relaxation of the spatial distribution of the scavenger around an OH.[97] The quantity $\beta$ is $5.6 \times 10^{-7}$ $s^{1/2}$ for the reaction of ethanol with OH, but $\beta$ is $2.4 \times 10^{-6}$ $s^{1/2}$ for the reaction of $Br^-$ with OH.[42] This difference reflects the much higher reactivity of OH with $Br^-$ compared to ethanol. The two scavenger species have similar diffusion coefficients. Usually the time dependence of a scavenging rate coefficient does not seriously affect the scavenging capacity dependence of yields, but the $\beta$ coefficient for $Br^-$ is particularly large.[42] There is no effect for small *s*, that is, scavenging at long times. Simulations for ethanol as the scavenger for OH are also included in Figure 8b, and the results of these calculations are in excellent agreement with the experimental data. Table 2 contrasts the effects of $Br^-$ and ethanol at a scavenging capacity

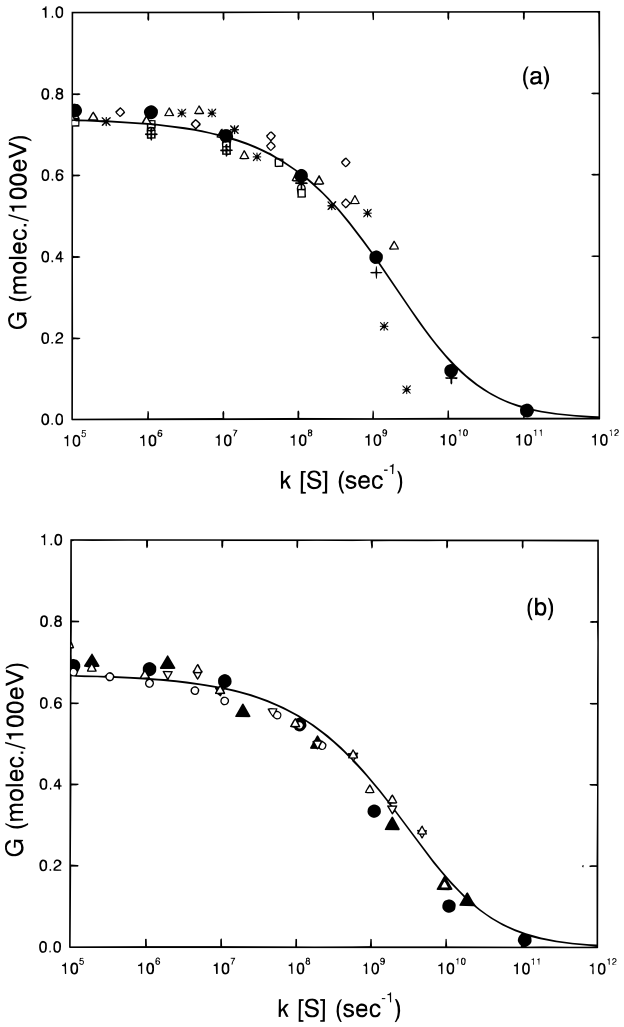


**Figure 8.** Scavenging capacity dependence of the scavenged yield of $H_2O_2$. (a) Scavenger experiments for pH 2: ref 90, $Br^-$ (□); ref 89, $Cl^-$ (◇); ref 91, $Br^-$ (○); ref 92, $Br^-$ (+); ref 93, EtOH (△), PrOH (*). Best fit to scavenger data is with $G_{esc} = 0.77$, $G_0 = 0.0$, and $\tau = 0.48$ ns. IRT simulation with $\sigma(e_{aq}^-) = 4.0$ nm and $\sigma(OH) = 0.75$ nm (●). (b) Scavenger experiments for pH 7: ref 91, $Br^-$ (○); ref 93, EtOH + $10^{-3}$ M $Me_2CO$ (△); ref 94, EtOH (▽). Best fit to scavenger data is with $G_{esc} = 0.67$, $G_0 = 0.0$, and $\tau = 0.13$ ns. IRT simulation with $\sigma(e_{aq}^-) = 4.0$ nm and $\sigma(OH) = 0.75$ nm with aerated $Br^-$ (●) and EtOH + $10^{-3}$ M $Me_2CO$ (▲).

**TABLE 2: Effects of Different Scavengers on the Yield of $H_2O_2$ and the Scavenging of OH in Solutions with the Same Scavenging Capacity for OH**

| solution | scavenging capacity for OH/s$^{-1}$ | calcd $G(H_2O_2)$ | measured $G(H_2O_2)$ | $G(\Delta OH)$ |
|---|---|---|---|---|
| 5 M ethanol | $0.95 \times 10^{10}$ | 0.150 | | 5.07 |
| 5 M ethanol + $10^{-3}$ M acetone | $0.95 \times 10^{10}$ | 0.153 | 0.152 [93] | 5.09 |
| 1.0 M bromide | $1.1 \times 10^{10}$ | 0.095 | | 5.32 |
| aerated 1.0 M bromide | $1.1 \times 10^{10}$ | 0.101 | | 5.31 |

of about $10^{10}$ s$^{-1}$ on the scavenged yield of OH and the yield of $H_2O_2$. The effect of the time dependent rate coefficient on the yield of $H_2O_2$ is very significant, resulting in a difference of over 50%. In contrast, the effect on the yield of scavenged OH is very small, being less than 4%. Clearly, the use of $Br^-$ as a prototypical OH scavenger can lead to an overestimate of the reduction in the yield of $H_2O_2$ at high $s$ if care is not taken in the modeling. The good agreement between simulation and experiment for the yield of $H_2O_2$ suggests that $\sigma(OH) = 0.75$ nm is appropriate, cf. the smaller and larger widths that were also considered earlier.

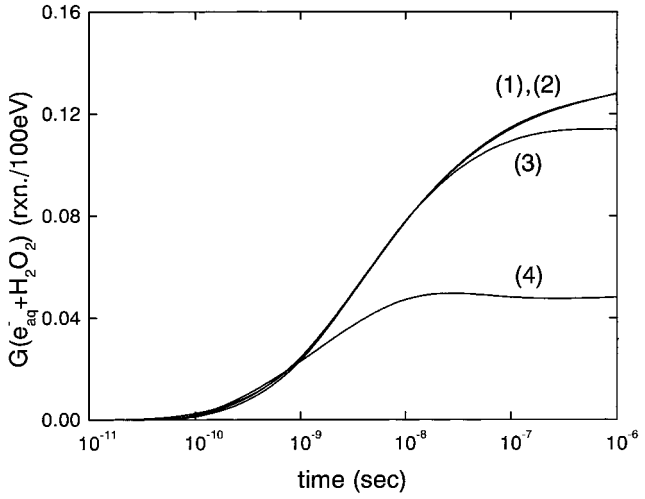


**Figure 9.** Time dependent kinetics of the reaction $e_{aq}^- + H_2O_2$ (reaction R8). IRT simulations with $\sigma(e_{aq}^-) = 4.0$ nm and $\sigma(OH) = 0.75$ nm shown as solid lines are labeled as follows: deaerated water (1); deaerated $10^{-5}$ M $Br^-$ (2); aerated $10^{-5}$ M $Br^-$ (3); $10^{-5}$ M $Br^-$ at pH 2 (4).

In a previous compilation[9] the two sets of data for the scavenging capacity dependence of the yield of $H_2O_2$ at pH 2 and pH 7 were presented together. This combination was inappropriate, since there is a considerable effect of pH on the yield of $H_2O_2$, cf. Figure 8. The experimental scavenger capacity dependence of the yield of $H_2O_2$ is accurately described by the empirical function (eq 2b) and the parameters $G_{esc} = 0.77$, $G_0 = 0.0$, and $\tau = 0.48$ ns at pH 2 and by $G_{esc} = 0.67$, $G_0 = 0.0$, and $\tau = 0.13$ ns at pH 7 (N.B., $p = 2s$). Changing the pH has little effect on the yield of reaction R7. The principal cause of the differences between the data at the two pHs is found in the reaction

$$e_{aq}^- + H_2O_2 \rightarrow OH + OH^- \qquad \text{(R8)}$$

This reaction leads to the destruction of the observed product (and the production of OH radical). The kinetics of reaction R8 in deaerated water and in solutions with a scavenging capacity for OH of $\sim 1 \times 10^5$ s$^{-1}$ is considered in Figure 9. The presence of a small concentration of OH scavenger does not affect the chemistry of reaction R8, since it scavenges only those OH radicals escaping the short-time nonhomogeneous stage in the development of the system. When the solution is aerated, the added solute scavenges $e_{aq}^-$. This reaction reduces the yield of reaction R8 by removing $e_{aq}^-$. However, the lifetime of $e_{aq}^-$ in aerated solution is ~200 ns. On this time scale, the yield of reaction R8 is still significant. The yield at 1 $\mu$s is 0.114 compared to 0.128 in deaerated solution. Thus, the presence of the $O_2$ or acetone has almost no influence on the yield of $H_2O_2$. At pH 2, the scavenging capacity of the solution for $e_{aq}^-$ is considerably larger than in aerated solution; the lifetime of $e_{aq}^-$ at pH 2 is ~4 ns, and consequently, the yield of reaction R8 is reduced to 0.048, less than about half that in aerated solution. The destruction of $H_2O_2$ via reaction R8 accounts for a reduction of 16% in the $G$ value at 1 $\mu$s compared to that expected from the yield of reaction R7. (In the experiments of ref 93, $10^{-3}$ M acetone is included as a scavenger for $e_{aq}^-$. The lifetime of $e_{aq}^-$ in $10^{-3}$ M acetone solution is ~150 ns, so the effect on the chemistry of the production of $H_2O_2$ is similar to that observed for aeration.)

The use of a spatial distribution with $\sigma(OH) = 0.75$ nm is further justified by considering the formation kinetics of $H_2O_2$

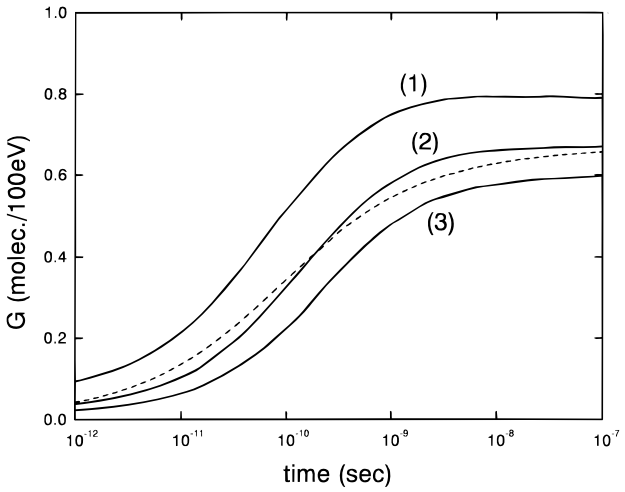


**Figure 10.** Time dependent formation of $H_2O_2$ in the electron radiolysis of water. ILT of best fit to experimental scavenger data at pH 7 with $G_{esc} = 0.67$, $G_0 = 0.0$, and $\tau = 0.13$ (dashed line). IRT simulations with $\sigma(e_{aq}^-) = 4.0$ nm shown as solid lines labeled as follows: $\sigma$(OH) = 0. 5 nm (1); $\sigma$(OH) = 0.75 nm (2); $\sigma$(OH) = 1.0 nm (3).

in water and comparing simulated kinetics and the inverse Laplace transform (ILT) kinetics predicted by the empirical function (eq 3) with the best fit parameters obtained from the scavenger experiments at pH 7. Figure 10 shows the ILT result (analyzed using a time dependent scavenging rate coefficient) and the results of simulations with $\sigma(e_{aq}^-) = 4.0$ nm and $\sigma$(OH) = 0.5, 0.75, and 1.0 nm. The best agreement is found for the simulations with $\sigma$(OH) = 0.75 nm.

**4.6. Spur Parameters**. It is appropriate to consider the physical implications of the local, or spur, distributions of $e_{aq}^-$ and of the heavier reactants, OH and $H_3O^+$. As discussed earlier, the relative separation of $e_{aq}^-$ and its sibling reactants OH and $H_3O^+$ essentially determines the decay kinetics of the $e_{aq}^-$, since the chemistry of $e_{aq}^-$ is controlled by reactions R1 and R2. These reactions have microsecond $G$ values of 0.6 and 1.2, respectively, compared to a total $G(\Delta e_{aq}^-)$ of ~2.4. For the Gaussian distributions employed here, the relative separation of an $e_{aq}^-$ and its sibling reactants is a Gaussian of standard deviation $(\sigma^2(e_{aq}^-) + \sigma^2(OH))^{1/2} \approx 4.1$ nm. This separation is primarily determined by the distribution for $e_{aq}^-$ with $\sigma(e_{aq}^-) = 4.0$ nm. The clear implication of this result is that $\sigma(e_{aq}^-)$ mainly represents the thermalization of the subexcitation electron. Additional evidence is the fact that the value of $\sigma(e_{aq}^-)$ is not affected by the choice of $\gamma_{final} = 5$ or 25 eV; in other words, the local spatial distribution of $e_{aq}^-$ within a spur is due mainly to the slowing of the low-energy electron from 5 eV to thermal energies or the trapping processes that occur concomitantly. There is a significant difference between the thermalization distributions derived here and the spur standard deviation obtained in deterministic calculations.[9,31,98,99] These calculations considered either a track-averaged isolated spur[9,98,99] or a distribution of isolated spurs[31] and were unable to faithfully reproduce both the observed decay kinetics of $e_{aq}^-$ and the scavenger concentration studies of $e_{aq}^-$, OH, $H_2$, and $H_2O_2$. This is also true of previous stochastic studies employing a distribution of isolated spurs.[38] The present track calculations consider realistic electron tracks, not spatially and chemically isolated spurs, and correctly incorporate the proximity of adjacent energy loss events and clusters of reactants. When calculations are performed using "isolated spur" distributions obtained from Monte Carlo track-simulated tracks with the widths obtained here, the modeled kinetics are in considerable error. (The spur size distribution is obtained by setting the overlap time to 1 ps and is found to be very similar to that predicted by analytic analysis of the energy loss distribution.[20]) Narrower spur widths on the order of 2−3 nm do permit agreement with some, but not all, of the experimental data. Effects due to the proximity of spurs are completely ignored in both deterministic and stochastic "isolated spur" calculations, and these effects have a significant influence on the observed experimental chemistry of water.

In contrast to $e_{aq}^-$, the chemistry of OH is dominated by reactions R2 and R7 with the latter making the greater contribution; the calculated microsecond $\Delta G$(OH) values are 1.2 and 1.6, respectively. The formation of $H_2O_2$ (and the decay of OH) is strongly influenced by the relative separations of OH radicals, that is, the value of $\sigma$(OH). Consequently, the initial spatial distribution of OH reflects a combination of the distance traveled by a low-energy electron of $E \approx \gamma_{final}$ before it undergoes a (terminal) electronic collision, i.e., the distance between the two nearest neighbor electronic collisions, and of the fragmentation distribution of the highly reactive molecular ion $H_2O^+$, which is the parent of OH. The root-mean-square distance between two OH radicals originating in the slowing down of a 25 eV electron is $\sigma(OH)\sqrt{6} \approx 1.8$ nm. This distance is considerably smaller than the calculated mean free path between electronic collisions for a 25 eV electron (~20 nm). However, at 25 eV the cross section for elastic collisions dominates that for inelastic collisions; the ratio $\sigma_{elastic}$:$\sigma_{inelastic}$ is ~9:1. When the degradation of the electron is simulated to $\gamma_{final} = 5$ eV, the average nearest event distance is of similar size to the root-mean-square distance between OH radicals using a Gaussian distribution of standard deviation 0.75 nm. It should be noted that cross sections are questionable below 25 eV and quantitative comments regarding the slowing of such low-energy electrons have to be viewed with caution.

## 5. Conclusions

Detailed stochastic modeling studies have been presented for the electron radiolysis of water and aqueous systems. Agreement between calculation and experimental data implies that the most important input in such modeling studies is the initial configuration of the reactants. The spatial distribution of reactants is determined by the structure of the radiation track and, therefore, by the energy loss properties of the electron in the medium of interest.

Comparison of the experimental data for the time dependent yield of $e_{aq}^-$ and the scavenging capacity dependence of the scavenged yield of $e_{aq}^-$ with stochastic diffusion−kinetic simulation shows a "thermalization" distribution for $e_{aq}^-$ of $\sigma \approx 4$ nm. This value is in good agreement with picosecond laser studies of the photoionization of water and with photoelectron ejection studies. Calculations for the formation of $H_2$ also agree with experimental yields. Detailed examination of the simulation results reveals that (at pH 7) the $H_2$ formed by nonhomogeneous reaction as opposed to unimolecular processes is due to the reactions $(e_{aq}^- + e_{aq}^-)$ and $(e_{aq}^- + H)$. The time scales of the two reactions differ by about a factor of 2, although they contribute equally to the yield of $H_2$ in water radiolysis.

Calculations for the radiation-induced chemistry leading to the formation of $H_2O_2$ are in agreement with experimental data. These calculations show the importance of the secondary reaction $(e_{aq}^- + H_2O_2)$ in determining the observable yield of $H_2O_2$. In aerated water, where homogeneous reaction is prevented, the yield of the reaction is ~0.12. Even in water at pH 2 where the lifetime of $e_{aq}^-$ is only ~4 ns, the yield is only reduced by 70%. Uncertainties concerning the experimental yield of OH make detailed comparisons with calculation difficult. The results reported here are consistent with the

available data, reproducing both the decay kinetics and the yields in scavenger experiments.

Although the calculations presented describe most of the experimental data, there are still discrepancies within the experimental data that the model cannot address. It is hoped, however, that the model will highlight these discrepancies and lead to further examination of some of these chemical systems.

**Acknowledgment.** The research described was supported by the Office of Basic Energy Sciences of the U.S. Department of Energy. This is Contribution NDRL-3968 of the Notre Dame Radiation Laboratory.

## References and Notes

(1) Pimblott, S. M.; Green, N. J. B. *Recent advances in the kinetics of radiolytic processes*; Compton, R. G., Hancock, G., Eds.; Elsevier: Amsterdam, 1995; Vol. 3, pp 117−174.
(2) Buxton, G. V. *Proc. R. Soc. London* **1972**, *A328*, 9−21.
(3) Fanning, J. E. Evidence for spurs in aqueous radiation chemistry. Ph.D. Thesis, University of Delaware, 1975.
(4) Jonah, C. D.; Miller, J. R. *J. Phys. Chem.* **1977**, *81*, 1974−1976.
(5) Jonah, C. D.; Matheson, M. S.; Miller, J. R.; Hart, E. J. *J. Phys. Chem.* **1976**, *80*, 1267−1270.
(6) Jonah, C. D.; Hart, E. J.; Matheson, M. S. *J. Phys. Chem.* **1973**, *77*, 1838−1843.
(7) Sumiyoshi, T.; Tsugaru, K.; Yamada, T.; Katayama, M. *Bull. Chem. Soc. Jpn.* **1985**, *58*, 3073−3075.
(8) Wolff, R. K.; Bronskill, M. J.; Aldrich, J. E.; Hunt, J. W. *J. Phys. Chem.* **1973**, *77*, 1350−1355.
(9) LaVerne, J. A.; Pimblott, S. M. *J. Phys. Chem.* **1991**, *95*, 3196−3206.
(10) Pimblott, S. M.; LaVerne, J. A. *Radiat. Res.* **1992**, *129*, 265−271.
(11) Mozumder, A.; Magee, J. L. *J. Chem. Phys.* **1966**, *45*, 3332−3341.
(12) Pimblott, S. M.; LaVerne, J. A.; Mozumder, A.; Green, N. J. B. *J. Phys. Chem.* **1990**, *94*, 488−495.
(13) LaVerne, J. A.; Pimblott, S. M. *Radiat. Res.* **1995**, *141*, 208−215.
(14) Pimblott, S. M.; LaVerne, J. A.; Mozumder, A. *J. Phys. Chem.* **1996**, *100*, 8595−8606.
(15) Nikjoo, H.; Goodhead, D. T.; Charlton, D. E.; Paretzke, H. G. *Phys. Med. Biol.* **1989**, *34*, 691−705.
(16) Goodhead, D. T.; Nikjoo, H. *Int. J. Radiat. Biol.* **1989**, *55*, 513−529.
(17) Nikjoo, H.; Goodhead, D. T.; Charlton, D. E. *Int. J. Radiat. Biol.* **1991**, *60*, 739−756.
(18) Goodhead, D. T.; Leenhouts, H. P.; Paretzke, H. G.; Terrissol, M.; Nikjoo, H.; Blaauboer, R. *Radiat. Prot. Dosim.* **1994**, *52*, 217−223.
(19) Nikogosyan, D. N.; Oraesky, A. A.; Rupasov, V. I. *Chem. Phys.* **1983**, *77*, 131−143.
(20) Pimblott, S. M.; Mozumder, A. *J. Phys. Chem.* **1991**, *95*, 7291−300.
(21) Inokuti, M. *Radiat. Res.* **1975**, *64*, 6−22.
(22) Long, F. H.; Lu, H.; Eisenthal, K. B. *Phys. Rev. Lett.* **1990**, *64*, 1469−1472.
(23) Long, F. H.; Lu, H.; Shi, X.; Eisenthal, K. B. *Chem. Phys. Lett.* **1991**, *185*, 47−52.
(24) Pimblott, S. M. *J. Phys. Chem.* **1991**, *95*, 6946−6951.
(25) Sander, M. U.; Luther, K.; Troe, J. *J. Phys. Chem.* **1993**, *97*, 11489−11492.
(26) Gauduel, Y.; Pommeret, S.; Migus, A.; Antonetti, A. *Chem. Phys.* **1990**, *149*, 1−10.
(27) Tan, K. H.; Brion, C. E.; van der Leeuw, P. E.; van der Wiel, M. J. *Chem. Phys.* **1978**, *29*, 299−309.
(28) Turner, J. E.; Magee, J. L.; Wright, H. A.; Chatterjee, A.; Hamm, R. N.; Ritchie, R. H. *Radiat. Res.* **1983**, *96*, 437−449.
(29) Turner, J. E.; Hamm, R. N.; Wright, H. A.; Ritchie, R. H.; Magee, J. L.; Chatterjee, A.; Bolch, W. E. *Radiat. Phys. Chem.* **1988**, *32*, 503−510.
(30) Hill, M. A.; Smith, F. A. *Radiat. Phys. Chem.* **1994**, *43*, 265−280.
(31) Schwarz, H. A. *J. Phys. Chem.* **1969**, *73*, 1928−1937.
(32) Clifford, P.; Green, N. J. B.; Pilling, M. J. *J. Phys. Chem.* **1982**, *86*, 1322−1327.
(33) Clifford, P.; Green, N. J. B.; Oldfield, M. J.; Pilling, M. J.; Pimblott, S. M. *J. Chem. Soc., Faraday Trans.* **1986**, *82*, 2673−2689.
(34) Clifford, P.; Green, N. J. B.; Pilling, M. J.; Pimblott, S. M. *J. Phys. Chem.* **1987**, *91*, 4417−4422.
(35) Green, N. J. B.; Pimblott, S. M. *J. Phys. Chem.* **1990**, *94*, 2922−2926.
(36) Pimblott, S. M.; Green, N. J. B. *J. Phys. Chem.* **1992**, *96*, 9338−9348.
(37) Pimblott, S. M.; LaVerne, J. A. *Radiat. Res.* **1990**, *122*, 12−23.
(38) Clifford, P.; Green, N. J. B.; Pilling, M. J.; Pimblott, S. M.; Burns, W. G. *Radiat. Phys. Chem.* **1987**, *30*, 125−132.
(39) Green, N. J. B.; Pilling, M. J.; Pimblott, S. M.; Clifford, P. *J. Phys. Chem.* **1990**, *94*, 251−258.
(40) Zaider, M.; Brenner, D. J. *Radiat. Res.* **1984**, *100*, 245−256.
(41) Brenner, D. J.; Zaider, M. *Radiat. Prot. Dosim.* **1985**, *13*, 127−131.
(42) Pimblott, S. M. *J. Phys. Chem.* **1992**, *96*, 4485−4491.
(43) Pimblott, S. M.; LaVerne, J. A.; Bartels, D. M.; Jonah, C. D. *J. Phys. Chem.* **1996**, *100*, 9412−9415.
(44) Kaplan, I. G.; Miterev, A. M.; Sukhonosov, V. Y. *Radiat. Phys. Chem.* **1990**, *36*, 493−498.
(45) Chernovitz, A. C.; Jonah, C. D. *J. Phys. Chem.* **1988**, *92*, 5946−5950.
(46) Balkas, T. I.; Fendler, J. H.; Schuler, R. H. *J. Phys. Chem.* **1970**, *74*, 4497−4505.
(47) Wolff, R. K.; Aldrich, J. E.; Penner, T. L.; Hunt, J. W. *J. Phys. Chem.* **1975**, *79*, 210−219.
(48) Yoshida, H. *Radiat. Res.* **1994**, *137*, 145−151.
(49) Schmidt, K. H.; Han, P.; Bartels, D. *J. Phys. Chem.* **1995**, *99*, 10530−10539.
(50) Dainton, F. S.; Logan, S. R. *Trans. Faraday Soc.* **1965**, *61*, 715−22.
(51) Jha, K. N.; Ryan, T. G.; Freeman, G. R. *J. Phys. Chem.* **1975**, *79*, 868−870.
(52) Shiraishi, H.; Katsamura, Y.; Hiroishi, D.; Ishigure, K.; Washio, M. *J. Phys. Chem.* **1988**, *92*, 3011−3017.
(53) Crowell, R. A.; Bartels, D. M. *J. Phys. Chem.* **1996**, *100*, 17940−17949.
(54) Konovalov, V. V.; Raitsimring, A. M.; Tsvetkov, Y. D. *Radiat. Phys. Chem.* **1988**, *32*, 623.
(55) Konovalov, V. V.; Raitsimring, A. M. *Chem. Phys. Lett.* **1990**, *171*, 326−334.
(56) Goulet, T.; Patau, J. P.; Jay-Gerin, J.-P. *J. Phys. Chem.* **1990**, *94*, 7312−7316.
(57) Goulet, T.; Jay-Gerin, J.-P. *J. Phys. Chem.* **1988**, *92*, 6871.
(58) Goulet, T.; Jay-Gerin, J.-P. *Radiat. Res.* **1989**, *118*, 46−62.
(59) Michaud, M.; Sanche, L. *Phys. Rev.* **1987**, *A36*, 4672−4683.
(60) Michaud, M.; Sanche, L. *Phys. Rev. A.* **1987**, *A36*, 4684−4699.
(61) Bader, G.; Chiasson, J.; Caron, L. G.; Michaud, M.; Sanche, L. *Radiat. Res.* **1988**, *114*, 467−479.
(62) Green, N. J. B.; Pimblott, S. M. *Mol. Phys.* **1991**, *74*, 795−810.
(63) Green, N. J. B.; Pimblott, S. M. *Mol. Phys.* **1991**, *74*, 811−832.
(64) Pimblott, S. M.; LaVerne, J. A. *J. Phys. Chem.* **1992**, *96*, 746−752.
(65) Jonah, C. D. *J. Phys. Chem.* **1974**, *78*, 2103−2105.
(66) Buxton, G. V.; Greenstock, C. L.; Helman, W. P.; Ross, A. B. *J. Phys. Chem. Ref. Data* **1988**, *17*, 513−886.
(67) Anbar, M.; Hart, E. J. *J. Phys. Chem.* **1965**, *69*, 1244−1247.
(68) Head, D. A.; Walker, D. C. *Can. J. Chem.* **1967**, *45*, 2051−2058.
(69) Keene, J. P. *Radiat. Res.* **1964**, *22*, 1−13.
(70) Hart, E. J.; Fielden, E. M. *Adv. Chem. Ser.* **1965**, *50*, 253−262.
(71) Janata, E.; Schuler, R. H. *J. Phys. Chem.* **1982**, *86*, 2078−2084.
(72) Elliot, A. J. *Radiat. Phys. Chem.* **1989**, *34*, 753−758.
(73) Anbar, M.; Neta, P. *Int. J. Appl. Radiat. Isot.* **1967**, *18*, 493−523.
(74) Koulkes-Pujo, A. M.; Michael, B. D.; Hart, E. J. *Radiat. Phys. Chem.* **1971**, *3*, 333−344.
(75) Pimblott, S. M.; LaVerne, J. A. *J. Phys. Chem.* **1992**, *96*, 8904−8909.
(76) Abramowitz, M.; Stegun, I. A. *Handbook of Mathematical Functions*; Dover: New York, 1970.
(77) Hunt, J. W.; Wolff, R. K.; Bronskill, M. J.; Jonah, C. D.; Hart, E. J.; Matheson, M. S. *J. Phys. Chem.* **1973**, *77*, 425−426.
(78) Schwarz, H. A. *J. Am. Chem. Soc.* **1955**, *77*, 4960−4964.
(79) Ghormley, J. A.; Hochanadel, C. J. *Radiat. Res.* **1955**, *3*, 227.
(80) Peled, E.; Czapski, G. *J. Phys. Chem.* **1970**, *74*, 2903−2911.
(81) Dixon, R. S. *Radiat. Res. Rev.* **1970**, *2*, 237−296.
(82) Armstrong, D. A. *The radiation chemistry of gases*; Farhataziz, Rodgers, M. A. J., Ed.; VCH Publishers: New York, 1987.
(83) Schuler, R. H.; Behar, B. *Scavenging studies of OH reactions in radiation tracks*; Dobo, J., Hedvig, P., Schiller, R., Eds.; Aksdemi Kiado: Budapest, 1983.
(84) Hart, E. J. *J. Am. Chem. Soc.* **1954**, *76*, 4198−4201.
(85) Draganic, I. G.; Nenadovic, M. T.; Draganic, Z. D. *J. Phys. Chem.* **1969**, *73*, 2564−2571.
(86) Draganic, I. G.; Draganic, Z. D. *J. Phys. Chem.* **1973**, *77*, 765−772.
(87) Burns, W. G.; Sims, H. E. *J. Chem. Soc., Faraday Trans. 1* **1981**, *77*, 2803−2813.
(88) LaVerne, J. A. *J. Phys. Chem.* **1988**, *92*, 2808−2809.
(89) Sworski, T. J. *Radiat. Res.* **1955**, *2*, 26−32.
(90) Sworski, T. J. *J. Am. Chem. Soc.* **1954**, *76*, 4687−4692.
(91) Allen, A. O.; Holroyd, R. A. *J. Am. Chem. Soc.* **1955**, *77*, 5852−5855.
(92) Rafi, A.; Sutton, H. C. *Trans. Faraday Soc.* **1965**, *61*, 877−890.

(93) Draganic, Z. D.; Draganic, I. G. *J. Phys. Chem.* **1969**, *73*, 2571−2577.
(94) Draganic, Z. D.; Draganic, I. G. *J. Phys. Chem.* **1971**, *75*, 3950−3957.
(95) Hong, K. M.; Noolandi, J. *J. Chem. Phys.* **1978**, *68*, 5172−5176.
(96) Hong, K. M.; Noolandi, J. *J. Chem. Phys.* **1978**, *68*, 5163−5171.
(97) Rice, S. E. *Diffusion-limited Reactions*; Rice, S. E., Ed.; Elsevier: Amsterdam, 1985; Vol. 25.
(98) Trumbore, C. N.; Short, D. R.; Fanning, J. E., Jr.; Olson, H. *J. Phys. Chem.* **1978**, *82*, 2762−2767.
(99) Burns, W. G.; Sims, H. E.; Goodall, J. A. B. *Radiat. Phys. Chem.* **1984**, *23*, 143−180.